Control Properties of Bottom Fired Marine Boilers

Solberg, Brian Willum; Andersen, Palle; Karstensen, Claus M. S.

Publication date:
2005

Document Version
Publisher's PDF, also known as Version of record

CONTROL PROPERTIES OF BOTTOM FIRED MARINE BOILERS

Brian Solberg and Claus M. S. Karstensen
Aalborg Industries A/S
9100 Aalborg, Denmark
Palle Andersen
Dept. of Control Engineering, Aalborg University
9220 Aalborg Øst, Denmark

ABSTRACT

This paper focuses on model analysis of a dynamic model of a bottom fired one-pass smoke tube boiler. Linearised versions of the model are analysed to determine how gain, time constants and right half plane zeros (caused by the shrink-and-swell phenomenon) depend on the steam flow load. Furthermore the interactions in the system are inspected to analyse potential benefit from using a multivariable control strategy in favour of the current strategy based on single loop theory.
An analysis of the nonlinear model is carried out to further determine the nonlinear characteristics of the boiler system and to verify whether nonlinear control is needed.
Finally a controller based on single loop theory is used to analyse if input constraints become active when rejecting transient behaviour from the disturbance steam flow.
The model analysis shows large variations in system gains at steady state as function of load whereas gain variations at the crossover frequency are small. Furthermore the interactions in the system prove not to be negligible and a subsequent controller design should take this into account using either Multiple input Multiple output control or Single input Single output controllers supported by a dynamical decoupling.
The results indicate that input constraints will become active when the controller responds to transients in the steam flow disturbance. For this reason an MPC (model predictive control) strategy capable of handling constraints on states and control signals should be considered. Furthermore hard constraint on the level variations also supports the choice of this strategy.
Keywords: Marine boiler, Dynamic models, Load dependency, Interaction, RGA, RIM, Decentralised control, Model nonlinearities

NOMENCLATURE

Symbol	Description
d, $\mathbf{d}$	disturbance (scalar/vector)
D, $\mathbf{D}$	scaling factor (scalar/matrix)
e, $\mathbf{e}$	error (scalar/vector)
k	valve conductance $\left[\frac{\text{kg}}{\text{s}\sqrt{\text{Pa}}}\right]$
L	level [m]
$\dot{m}$	mass flow $\left[\frac{\text{kg}}{\text{s}}\right]$
P	pressure [Pa]
r	reference
T	temperature [°C]
u, $\mathbf{u}$	input (scalar/vector)
x, $\mathbf{x}$	state (scalar/vector)
y, $\mathbf{y}$	output (scalar/vector)
κ	RIM
$\mathbf{\Lambda}$	RGA
Subscripts	**Description**
b	bobbles
f	flue gas
fw	feed water
fu	fuel
m	metal
s	steam
w	water
Abbreviations	**Description**
MIMO	multiple input multiple output
MPC	model predictive control
ORG	origin
PI	proportional and integral
RGA	relative gain array
RHP	right half plane
RIM	Rijnsdorp interaction measure
SISO	single output single input

INTRODUCTION

During the years marine boilers have been controlled using classical SISO controllers. Lately focus has been put on optimising the boiler performance through a more comprehensive and coherent control

strategy. This includes model-based MIMO control to minimise variation in especially drum water level. With this parameter minimised it is possible to reduce the physical dimensions of the boiler which imply lower production costs and gives a more competitive product.
Prior to setting up a control strategy it is important to understand the process to be controlled and the model describing it. The boiler system is nicely described by means of first principles resulting in a model based on nonlinear differential equation, see e.g. [1] and [2]. This model has a MIMO structure meaning that all process inputs affect all the outputs. It is of interest to know how large the interactions in the MIMO system are and also the degree of nonlinearities in the model and if any of these properties will affect the controlled boiler system.
The model which is analysed in this paper is based on the bottom fired one-pass smoke tube boiler (MISSION^{TM} OB) from Aalborg Industries A/S product range. The largest of these has a maximum steam load of 3000 $\frac{\text{kg}}{\text{h}}$.
The paper starts by introducing the boiler model and deriving linear versions of this depending on the operating point. After that follows the analysis based on mostly linear system theory using the concept of decentralised control and decoupling to find interaction.

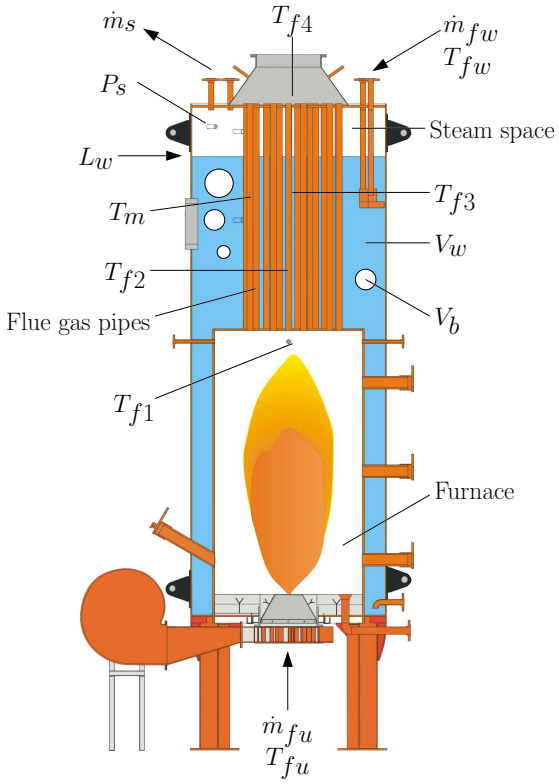

Figure 1: Drawing of the bottom fired one-pass smoke tube boiler.

BOILER MODEL

A drawing of the bottom fired one-pass smoke tube boiler is shown in figure 1 with model variables indicated. A model of this boiler was presented in [2]. The model has the structure:

$$\mathbf{F}(\mathbf{x})\dot{\mathbf{x}} = \mathbf{h}(\mathbf{x},\mathbf{u},\mathbf{d}) \quad (1)$$
$$\mathbf{y} = \mathbf{c}(\mathbf{x}) \quad (2)$$

where $\mathbf{u} = [\dot{m}_{fu}, \dot{m}_{fw}]^T$ (fuel flow and feed water flow), $\mathbf{y} = [P_s, L_w]^T$ (steam pressure and water level), $\mathbf{d} = [k, T_{fu}, T_{fw}]^T$ ("steam flow", fuel temperature and feed water temperature) and $\mathbf{x} = [T_{f1}, T_{f2}, T_{f3}, T_{f4}, T_m, P_s, V_w, V_b]^T$ (T_f being temperatures at four different levels in the furnace and convection parts, T_m is the temperature of the metal separating the heating part and the liquid part and V_w and V_b are volumes of water and steam bobbles under the surface in the drum).
It should be mentioned here that the disturbance k is related to the actual steam flow as $\dot{m}_s = k\sqrt{P_s - P_{atm}}$, and can be interpreted as an overall steam valve and pipe system conductance. k will also be referred to as the steam flow disturbance. P_{atm} is the atmospheric pressure at the pipe outlet.
A parameter estimation was made to find the critical parameters in the model in such a way that it reflects the physical boiler system as well as possible.

Linear Model

Linearised versions of the plant are introduced as most of the model analysis and controllers designed will be based on these. The linearisation is based on a first order Taylor series expansion. Scaling of the models is introduced (according to Skogestad and Postlethwaite [3]) as it makes both model analysis and controller design simpler.
Let the unscaled linear small signal valued plant model including tracking error in the Laplace domain be given as:

$$\check{\mathbf{y}}(s) = \check{\mathbf{G}}_u(s)\check{\mathbf{u}}(s) + \check{\mathbf{G}}_d(s)\check{\mathbf{d}}(s) \quad (3)$$
$$\check{\mathbf{e}}(s) = \check{\mathbf{r}}(s) - \check{\mathbf{y}}(s) \quad (4)$$

Introduce scaling factors put up from system demands; allowable control error, knowledge of disturbance variations and allowable input change e.g. due to valve opening constraints or maximal flow rate etc.:

$$D_{e,i} = \check{e}_{max,i}, \quad D_{u,j} = \check{u}_{max,j}, \quad D_{d,k} = \check{d}_{max,k}$$

where the subscripts i, j, k represent the different numbers of entries in the error, input and disturbance

vector respectively. The specific values are listed below:

	$\check{e}_{max}$	$\check{u}_{max}$	$\check{d}_{max}$
1	0.5 bar	160 $\frac{\text{kg}}{\text{g}}$	$6.0 \cdot 10^{-4}$ $\frac{\text{kg}}{\text{s}\sqrt{\text{Pa}}}$
2	0.1 m	4500 $\frac{\text{kg}}{\text{g}}$	5 °C
3			5 °C

The value of $\check{d}_{max,1} = k_{max}$ is determined from assuming a maximal steam flow of 3000 $\frac{\text{kg}}{\text{h}}$, a steam flow range of 40-100% and assuming that steps in the flow from maximum to minimum and the opposite can occur.
Using vector notation, putting the scaling element on the diagonal of a scaling matrix, the scaled output, input, disturbance and reference vectors are given as:

$$\mathbf{y} = \mathbf{D}_e^{-1}\check{\mathbf{y}}, \quad \mathbf{u} = \mathbf{D}_u^{-1}\check{\mathbf{u}}$$
$$\mathbf{d} = \mathbf{D}_d^{-1}\check{\mathbf{d}}, \quad \mathbf{r} = \mathbf{D}_e^{-1}\check{\mathbf{r}}$$

Substituting these scaled vector representations into equations 3 and 4 gives the scaled model:

$$\begin{aligned} \mathbf{y}(s) &= \mathbf{G}_u(s)\mathbf{u}(s) + \mathbf{G}_d(s)\mathbf{d}(s) \qquad (5) \\ \mathbf{e}(s) &= \mathbf{r}(s) - \mathbf{y}(s) \end{aligned}$$

where $\mathbf{G}_u(s) = \mathbf{D}_e^{-1}\check{\mathbf{G}}_u(s)\mathbf{D}_u$ and $\mathbf{G}_d(s) = \mathbf{D}_e^{-1}\check{\mathbf{G}}_d(s)\mathbf{D}_d$.
Now $\|\mathbf{d}(t)\|_\infty \leq 1$ and the objective is to keep $\|\mathbf{e}(t)\|_\infty \leq 1$ while obeying $\|\mathbf{u}(t)\|_\infty \leq 1$. If needed additional scaling can be applied to the references to keep $\|\mathbf{r}(t)\|_\infty \leq 1$ during reference changes.

Actuator Models

In the aforementioned boiler model the actuator dynamics were omitted. The actuators will enter in the closed loop strategy in a cascade configuration. The actuators used for both the fuel and feed water flow are valves with a pneumatic actuation. Measurements show that these have a rise time from control signal to flow of $t_r < 10$ s. It is assumed that cascade controllers linearising the actuator dynamics can be designed with a dynamic behaviour equal to or faster than the open loop actuator dynamics.
Models of the controlled actuators with reference flows as input and actual flows as output can be put in a matrix form as:

$$\mathbf{G}_a(s) = \begin{bmatrix} G_{a11}(s) & 0 \\ 0 & G_{a22}(s) \end{bmatrix}$$

Both controlled actuators are assumed to be well described by second order systems. Introducing this model in the total linear model gives a new transfer function from input to output: $\mathbf{G}(s) = \mathbf{G}_u(s)\mathbf{G}_a(s)$

MODEL ANALYSIS

During this analysis especially three operating points will be considered; minimum load: 40%, middle load: 70% and maximum load 100%. Expanding the notation of equation 5, including the actuator dynamics, illustrates the transfer functions of the model:

$$\begin{bmatrix} y_1 \\ y_2 \end{bmatrix} = \begin{bmatrix} G_{11} & G_{12} \\ G_{21} & G_{22} \end{bmatrix} \begin{bmatrix} u_1 \\ u_2 \end{bmatrix} + \\ + \begin{bmatrix} G_{d11} & G_{d12} & G_{d13} \\ G_{d21} & G_{d22} & G_{d23} \end{bmatrix} \begin{bmatrix} d_1 \\ d_2 \\ d_3 \end{bmatrix}$$

where the dependency of s is omitted. This will be done throughout the analysis, to simplify expressions, where this dependency is obvious. A block diagram illustration of the system is shown in figure 2. In

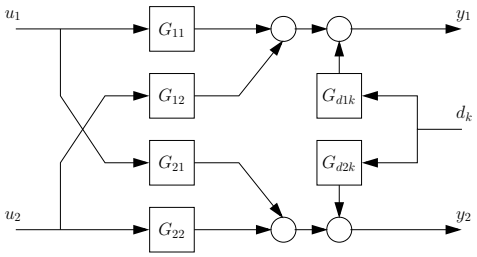

Figure 2: Block diagram of linear boiler model.

figure 3 a magnitude plot of the transfer functions of $\mathbf{G}(s)$ is presented for each of the three mentioned operating points.

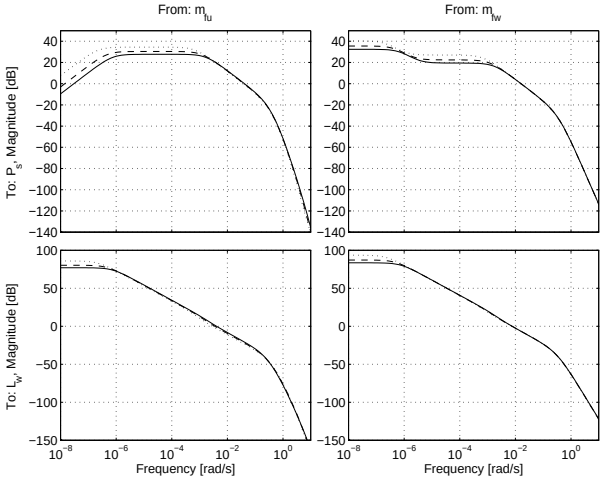

Figure 3: Magnitude plots of transfer functions in $\mathbf{G}(s)$ at three different loads; 100% solid, 70% dashed and 40% dotted.

The actual differences in model dynamics are not well visualised in these plots. In figure 4 magnitude plots

of $G_{ij,40}/G_{ij,100}$, the ratios between the transfer functions at 40% load and 100% load are shown.

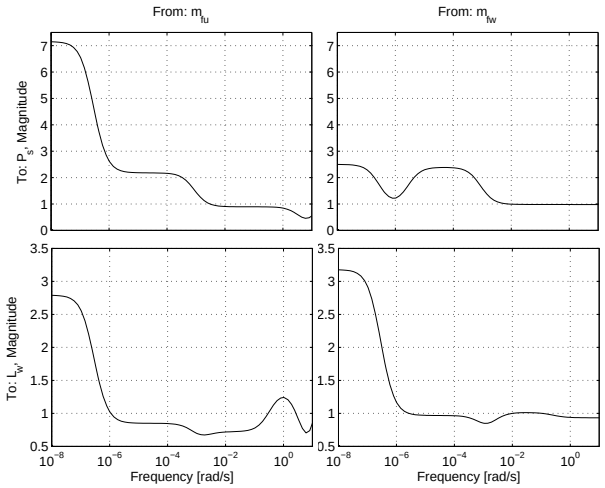

Figure 4: Magnitude plot of $G_{ij,40}/G_{ij,100}$.

From the plots it can be seen that the main differences between the model dynamics at the different operating points are at low frequencies where gain increases at lower load. On the other hand at frequencies above 10^{-3} rad/s for output one, P_s, and above 10^{-6} rad/s for output two, L_w, the behaviours are similar at least up to about 10 rad/s where the ratios associated with the fuel flow input break off. It is of interest to find out whether these differences have any practical implication in a controller design and furthermore whether interactions in the system should be handled by a MIMO control strategy.

It is obvious from the magnitude plots that they do not give any useful information regarding gains and time constants as both quantities are unreasonable high due to a pole in the left half plane close to the origin. Furthermore it can be seen that the steady state gain of $G_{11}(s)$ is zero indicating a zero in the origin.

Instead of looking at gains at steady state and at the usual definition of time constants another approach is taken. Focus is put at the crossover frequency ω_c. Assuming knowledge of this quantity at the operating point of 100% a suitable controller for this specific load can be designed. Now the system gain variations can be defined as the variations at the crossover frequency when the operating point is changed but the same controller is applied. Furthermore instead of considering the actual time constants the variations of the crossover frequency when the operating point is changed are investigated.

This approach gives insight to the stability properties of the nonlinear boiler system.

Decentralised Control

The controller designed is a simple decentralised controller using SISO PI controllers. An estimate of the bandwidth requirements without taking MIMO interaction into account are investigated from a plot of the magnitudes of the transfer functions from the disturbances to the output, $G_d(s)$, shown in figure 5.

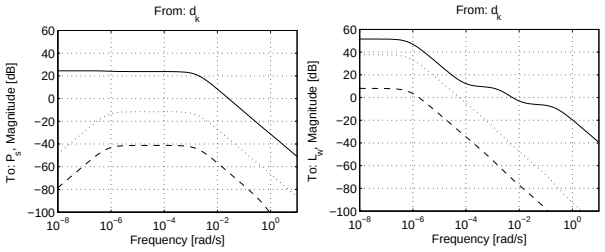

Figure 5: The left plot shows the magnitude plot from $\mathbf{d}$ to y_1 and the right plot the magnitude plot from $\mathbf{d}$ to y_2. The solid line is associated with d_1, the dashed line with d_2 and the dotted line with d_3.

Control is needed at frequencies where $|G_{dik}(j\omega)| > 1$, $|G_{dik}|$ being the disturbance gain from disturbance k to output i. From the plots it can be seen that for both the pressure, y_1 and water level, y_2, the worst disturbance is the change in the steam flow; disturbance d_1. The two temperature disturbances have proved to play a minor role in a closed loop configuration and will not be addressed further in this paper. G_{d11} cross the zero axis at $\omega_{b1} \approx 0.027$ rad/s and G_{d21} cross the zero axis at $\omega_{b2} \approx 0.006$ rad/s, setting an estimated bandwidth requirement for the pressure and level loop, respectively.

Stability conditions imposed by interaction

Of interest when performing model analysis and designing decentralised controllers are the stability conditions imposed by interactions in the MIMO model when using the diagonal controller.
Let $\mathbf{P}$ be a square $n \times n$ plant and let $\tilde{\mathbf{P}}$ ("nominal plant") be given as:

$$\tilde{\mathbf{P}} = \begin{bmatrix} P_{11} & 0 & \\ 0 & \ddots & 0 \\ & 0 & P_{nn} \end{bmatrix}$$

Then the closed loop system can be presented as in figure 6.
$\mathbf{K}$ is diagonal and $\mathbf{E}$ is an output multiplicative perturbation given as:

$$\mathbf{E} = (\mathbf{P} - \tilde{\mathbf{P}})\tilde{\mathbf{P}}^{-1}$$

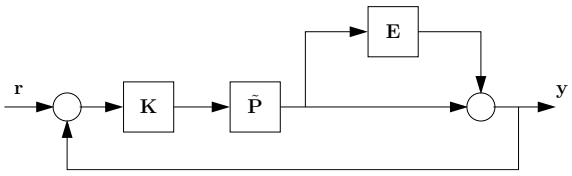

Figure 6: Block diagram of closed loop with $\mathbf{P}$ represented as the diagonal plant $\tilde{\mathbf{P}}$ and an output multiplicative perturbation $\mathbf{E}$.

By Skogestad [3] the overall output sensitivity function for this system can be factorised as:

$$\mathbf{S} = \tilde{\mathbf{S}}(\mathbf{I} + \mathbf{E}\tilde{\mathbf{T}})^{-1}$$

where $\tilde{\mathbf{S}} = (\mathbf{I} + \tilde{\mathbf{P}}\mathbf{K})^{-1}$ is the sensitivity function of the nominal system and $\tilde{\mathbf{T}} = \mathbf{I} - \tilde{\mathbf{S}}$.
Now assume that $\mathbf{P}$ is stable and furthermore that the individual loops are stable ($\tilde{\mathbf{S}}$ and $\tilde{\mathbf{T}}$ stable), then for stability of the overall system it suffices to look at

$$\det(\mathbf{I} + \mathbf{E}\tilde{\mathbf{T}}(s)) \tag{6}$$

as s traverses the Nyquist D-contour and make sure it does not encircle the origin. This follows from lemma A.5 in [3]. The spectral radius stability condition then yields stability of the overall system if:

$$\rho(\mathbf{E}\tilde{\mathbf{T}}(j\omega)) < 1 \ \forall\, \omega$$

2×2 **systems:** For these systems the condition becomes especially simple. This will be illustrated with the system addressed in this paper.

$$\mathbf{E} = \begin{bmatrix} 0 & \frac{G_{12}}{G_{22}} \\ \frac{G_{21}}{G_{11}} & 0 \end{bmatrix}, \ \tilde{\mathbf{T}} = \begin{bmatrix} \tilde{T}_{11} & 0 \\ 0 & \tilde{T}_{22} \end{bmatrix}$$

The spectral radius of $\mathbf{E}\tilde{\mathbf{T}}(j\omega)$ is given by:

$$\rho(\mathbf{E}\tilde{\mathbf{T}}(j\omega)) = \left| \sqrt{\tilde{T}_{11}\tilde{T}_{22}\kappa(j\omega)} \right|$$

where $\kappa = \frac{G_{12}G_{21}}{G_{11}G_{22}}$ is the RIM (Rijnsdorp interaction measure) introduced by Rijnsdorp [4]. Now the sufficient condition for stability of the overall system is:

$$|\tilde{T}_{11}\tilde{T}_{22}(j\omega)| < \frac{1}{|\kappa(j\omega)|} \ \forall\, \omega$$

or the more conservative condition:

$$|\tilde{T}_{ii}(j\omega)| < \frac{1}{\sqrt{|\kappa(j\omega)|}} \ \forall\, \omega, i \in [1,2]$$

Bounds can be set on the sizes of $\tilde{T}_{11}(j\omega)$ and $\tilde{T}_{22}(j\omega)$ according to their resonant peaks which again are related to the stability margins of the individual loops. This gives the more conservative condition:

$$\|\tilde{T}_{ii}\|_\infty < \frac{1}{\sqrt{|\kappa(j\omega)|}} \ \forall\, \omega, i \in [1,2] \tag{7}$$

Hence to ensure stability of a system with offset-free tracking ($T_{ii}(0) = 1$) assuming no resonant peaks the condition becomes $1 < 1/|\kappa(j\omega)| \ \forall\, \omega$. From equation 7 it follows that the interactions in the system pose no limit on the achievable closed loop system bandwidth if $\kappa < 1$.
It is obvious that systems with $|\kappa(j\omega)| \ll 1 \ \forall\, \omega$ are preferable. One could interpret the degree to which $\kappa < 1$ as an insurance of a good stability margin. This also relates to another measure of interaction; the relative gain array (RGA), first introduced by Bristol [5], which is given as

$$\mathbf{\Lambda}(\mathbf{G}(s)) = \mathbf{G}(s) \circ (\mathbf{G}^{-1}(s))^T$$

where $\circ$ is the element wise product (also known as the Schur or Hadamard product). In the following shortened to $\mathbf{\Lambda}(\mathbf{s})$. An element of the RGA, $\Lambda_{ij}(s)$, is the ratio between the gain of G_{ij} assuming all other loops open and the gain of G_{ij} assuming all other loops closed by perfect control. Both the RIM and the RGA are independent of the particular plant input and output scaling. For 2×2 systems the RGA can be expressed as:

$$\mathbf{\Lambda}(s) = \begin{bmatrix} \frac{1}{1-\kappa(s)} & \frac{-\kappa(s)}{1-\kappa(s)} \\ \frac{-\kappa(s)}{1-\kappa(s)} & \frac{1}{1-\kappa(s)} \end{bmatrix}$$

In most cases for stability of the overall system using diagonal decentralised control it is sufficient to require $\mathbf{\Lambda}(j\omega_c) \approx \mathbf{I}$ at the crossover frequencies [3], which is the same as requiring $|\kappa(j\omega_c)| \ll 1$. $\mathbf{\Lambda}(j\omega_c) = \mathbf{I}$ imply that the individual loops are independent of the closing of the other loops meaning that the stability margins from the individual loops are preserved. Furthermore a unity RGA implies that there are zero or only one way interaction. One way interaction can be interpret and treated as a disturbance.
In figure 7 $1/|\kappa(j\omega)|$ for $\mathbf{G}$ is plotted.

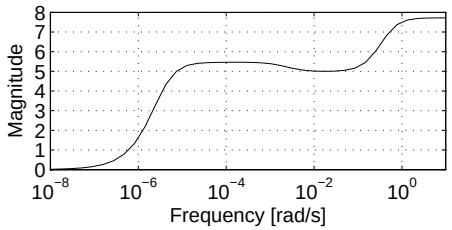

Figure 7: Plot of $1/|\kappa(j\omega)|$.

Now assume that $\tilde{T}_{ii}$ for all i is designed with no resonant peak such that $\|\tilde{T}_{ii}\|_\infty \leq 1$ given the sufficient

condition for stability: $1 < 1/|\kappa(j\omega)| \; \forall \omega$ then it is obvious from the figure 7 that stability is not ensured in the low frequency band. This is due to the zero in the origin of G_{11}. However the spectral radius stability condition is conservative meaning that this does not necessarily imply that the system is unstable.
To investigate whether the conditions in the low frequency band cause any stability problems for the overall loop again look at equation 6. Notice that at low frequencies $\tilde{\mathbf{T}} \approx \mathbf{I}$. This means that for overall stability it suffices to ensure that $\det(\mathbf{I} + \mathbf{E}(j\omega))$ behaves well at low frequencies (does not encircle the origin). Given this overall stability is ensured by (7) for $\|\tilde{T}_{ii}\|_\infty$ small enough. The Nyquist plot of $\det(\mathbf{I} + \mathbf{E}(j\omega))$ is shown in figure 8.

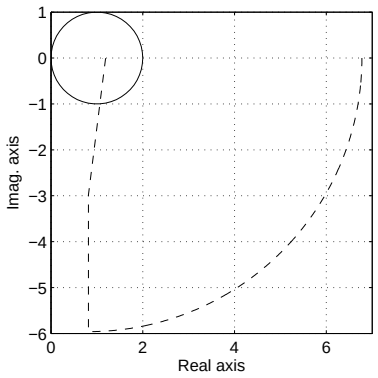

Figure 8: Nyquist plot of $\det(\mathbf{I} + \mathbf{E}(j\omega))$.

As can be seen the curve indeed behaves well at low frequencies and there are no encirclements of the origin. From the analysis it can be concluded looking at figure 7 (assuming $\tilde{\mathbf{T}}(j\omega) \approx \mathbf{I} \; \forall \omega < 10^{-5}$ for the previous analysis to hold) that to ensure stability of the overall system the condition is according to (7); $\|\tilde{T}_{ii}\|_\infty < \sqrt{5}$ that is a resonant peak less than $\sqrt{5}$. If $\tilde{T}_{ii}$ is assumed to have second order characteristics the resonant peak requirement can be related directly to the phase margins of $\tilde{T}_{ii}$ [6]. E.g. a resonant peak of $\sqrt{5}$ corresponds to a phase margin of approximately 26°.

Pairing

The RGA is often used as a measure for pairing control inputs to outputs as the structure of the RGA is dependent on this pairing. Recalling from the last section that to ensure stability one often requires that $\mathbf{\Lambda}(j\omega_c) \approx \mathbf{I}$, similar to requiring $1 \ll 1/|\kappa(j\omega_c)|$. From the discussion regarding the required bandwidth the crossover frequencies can be expected to be $\omega_{c1} > 0.027$ rad/s and $\omega_{c2} > 0.006$ rad/s. It can be seen from figure 7 that the current pairing (controlling pressure with fuel flow and water level with feed water flow) is the best choice, as would be expected. Intuitively pairing inputs and outputs for which $\Lambda_{ij} = 1$ also makes sense as this means that the gain seen from input j to output i is unaffected by the closing of the other loops.
However focusing on the low frequency range figure 7 shows that the chosen pairing results in small RGA elements indicating control problems if one loop breaks. The problem here is a zero in the origin of the transfer function $G_{11}(s)$ from fuel to pressure discussed below.

RHP-zeros

In SISO controller design and for process understanding it is of interest to determine possible non-minimum phase zeros in the process. Furthermore as discussed above zeros in the origin play a dominant role in the controller design.
A list of the transfer functions with either a RHP-zero or a zero in the origin (ORG-zero) is shown below.

RHP − zero	G_{12}	G_{21}	G_{d21}	G_{d22}	G_{d23}
ORG − zero	G_{11}	G_{d12}	G_{d13}		

In the following only the zeros most important to the analysis will be discussed.
The zero in the origin of $G_{11}(s)$ arises from the fact that with the boiler in steady state an increase in fuel input, keeping feed water flow constant, causes the steam flow to increase and the water level to drop. But as the water level drops efficiency drops. At some point the water level has dropped so much that the efficiency is so poor that the steam outlet is equal to the feed water input and a new equilibrium is found at the same pressure. In reality this new equilibrium will not appear due to the large system steady state gains meaning that the boiler will dry out. The zero may be removed by closing the water level loop. This means that if for some reason the level loop should break then difficulties in controlling the pressure could be expected. This was also the conclusion from the RGA analysis in the previous section.
Regarding the RHP-zeros the most interesting are the ones in the cross connections G_{12} and G_{21} and the one from steam flow to water level in G_{d21} which describes the shrink-and-swell phenomenon in the process. In fact the zero in G_{21} is closer to the origin than the zero in G_{d21} and furthermore it is associated with a larger gain.
Common for the RHP-zeros are that as the operating load drops the zeros move closer to the origin. Together with the increasing gain this makes the effect of these zeros most pronounced at low loads.
Seen from a control point of view the RHP-zeros do not pose any limits on performance as they are not present in $G_{11}(s)$ and $G_{22}(s)$. However it should

be mentioned that a RHP-zero was expected in the transfer function $G_{22}(s)$ from feed water to water level but so far no measurement have indicated this.

Loop Closing

As was noted previously the transfer function $G_{11}(s)$ has a zero in the origin, indicating that u_1, fuel flow, can not be used to control y_1, the pressure. However the RGA analysis showed a different result which calls for design via sequential loop closing. This technique also has the advantage of ensuring stability, though the performance of the inner loop might be disturbed when closing the outer loop [3].
PI controllers are used in both loops. These are designed to achieve the largest possible bandwidth in both loops having a phase margin of 45° well above the limit found previously.
First the level loop is closed using K_{22} as illustrated in figure 9. The new transfer function from u_1 to y_1 is given as:

$$y_1 = G_{11}\left(1 - \frac{\kappa}{\frac{1}{G_{22}K_{22}} + 1}\right) u_1 = G'_{11}u_1 \qquad (8)$$

Inspecting this equation it can be seen that at low frequencies: $G'_{11} \approx G_{11}(1-\kappa)$, as $G_{22}K_{22}$ is large at frequencies where feedback is effective. At high frequencies κ is small indicating that $G'_{11} \approx G_{11}$. As the controller design focuses on relatively high frequencies a design using G_{11} should be adequate though (8) is used to design K_{11}, due to slight phase differences between this and the approximation.

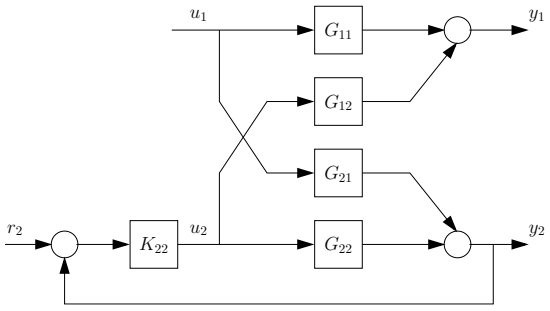

Figure 9: Level loop closed in the sequential design strategy.

Load dependency

Having determined two SISO controllers and thereby found the crossover frequency for both loops ($\omega_{c1} = 0.08$ rad/s $> \omega_{b1}$ and $\omega_{c2} = 0.13$ rad/s $> \omega_{b2}$) the load dependency of gains at the crossover frequencies and the variation of these crossover frequencies can be determined applying the controllers found for the 100% load at the remaining two operating points considered, 70% and 40%.
In the following it is assumed that the level loop is closed meaning that $G'_{11}(s)$ and not $G_{11}(s)$ is in focus. In figure 10 the mentioned variations as function of load are plotted. Included in the figure are also the variations of the stability margins.

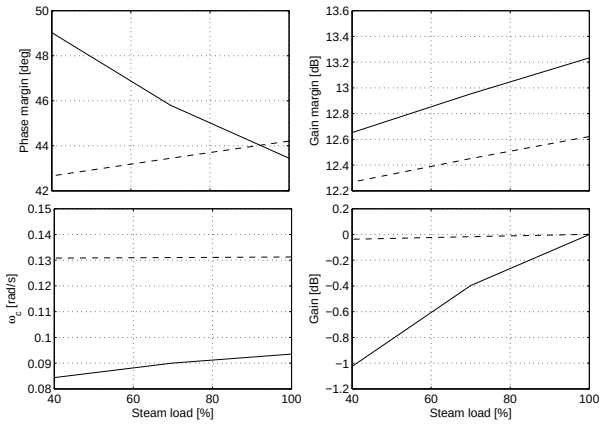

Figure 10: Plots of phase margin variations (top left), gain margin variations (top right), crossover frequency variations (bottom left) and variations of gain at the crossover frequencies for the loop at 100% load (bottom right) all as function of load. The solid line represents the loop associated with G'_{11} (pressure loop) and the dashed line the loop corresponding to G_{22} (level loop).

It is clear from the figure that nonlinearities in the model have most effect on the pressure loop. Nevertheless neither stability margins nor gains and crossover frequency vary remarkably over the load range considered.
To illustrate that the cross terms in the model do not cause the system to become unstable and to illustrate the little influence nonlinearities have on stability a Nyquist plot of $\det(\mathbf{I} - \mathbf{GK}(s))$ is shown in figure 11. The plot is shown for the three operating points under consideration given the same controller. From the right plot, focusing around the unit circle, it can be seen that stability is not effected by cross terms and nor by nonlinearities as the three curves cross the unit circle at the same point.

Model Nonlinearity

From figure 3 and the results above it is clear that the nonlinearities are mainly pronounced in the low frequency band as function of load. To investigate whether these low frequency variations should have any influence on the choice of control strategy (linear/nonlinear) the two SISO controllers developed in

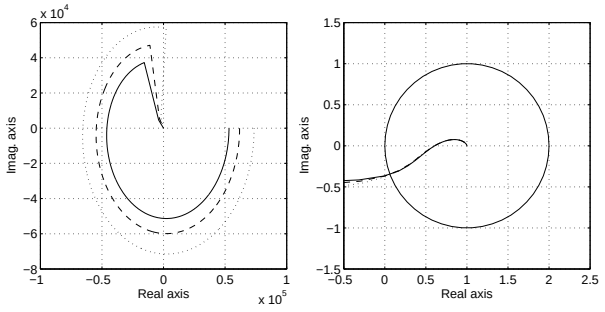

Figure 11: Nyquist plot of open loop system with controller base on sequential loop closing. Left: full plot, right: zoom around the unit circle. The solid line represents a linear model at 100% load, the dashed line a model at 70% load and the dotted line a model at 40% load.

the last section are simulated together with the nonlinear model. Steps in the steam flow disturbance, k, of different sizes are made starting from different operating points. To compare the responses the outputs are normed with the size of the disturbance step. The result is shown in figure 12.

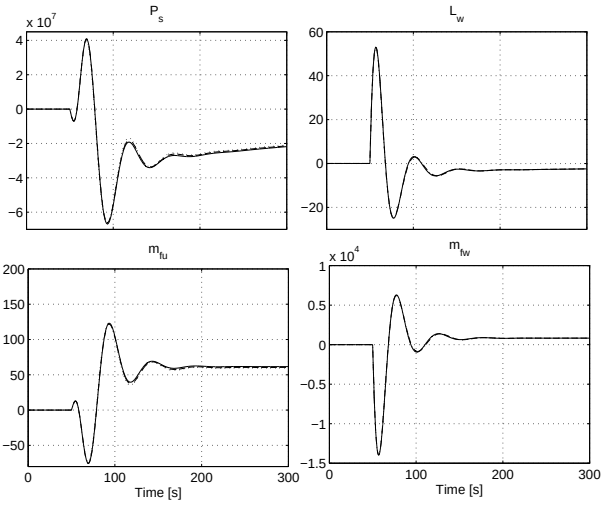

Figure 12: Closed loop response to step disturbance on nonlinear model. Three different step responses are shown; 50% $\rightarrow$ 75%, solid, 50% $\rightarrow$ 100%, dashed and 75% $\rightarrow$ 100%, dotted.

From the plots it can be seen that the transient behaviour for each step made is approximately the same. The largest differences in the plots are on pressure and fuel flow. This is illustrated in figure 13 where only the last 200 s of figure 12 is shown. Referring to figure 4 this makes sense as the largest gain variations over load are associated with the pressure.

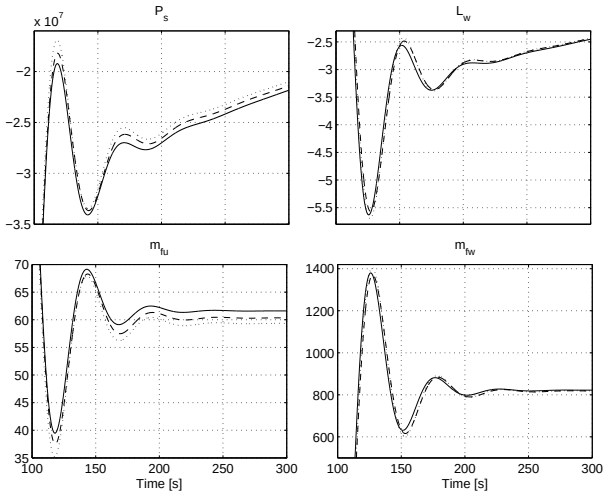

Figure 13: Figure 12 repeated with reduced axes.

Influence of interaction on performance

Having a MIMO system it is of interest to investigate the potential benefit from a MIMO controller design. This can be evaluated by inspecting the influence of the interactions in the model on the achievable controller performance, hereby meaning the ability of the controller to reject the disturbances.
The effect of the cross terms might be positive causing damping of the disturbances but amplification is also a possibility. To investigate this the performance of the previously designed controller will be compared to that of a controller designed after decoupling the interactions in the model. The decoupled system is illustrated in figure 14 assuming perfect decoupling.

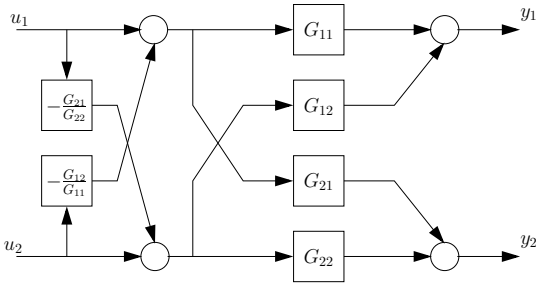

Figure 14: Decoupled system.

This system can be described as:

$$\mathbf{y} = \mathbf{G}^*\mathbf{u} = \mathbf{G}\mathbf{W}\mathbf{u}$$

where

$$\mathbf{W} = \begin{bmatrix} 1 & -\frac{G_{12}}{G_{11}} \\ -\frac{G_{21}}{G_{22}} & 1 \end{bmatrix}$$

giving the new system:

$$\begin{bmatrix} y_1 \\ y_2 \end{bmatrix} = \begin{bmatrix} G_{11}(1-\kappa) & 0 \\ 0 & G_{22}(1-\kappa) \end{bmatrix} \begin{bmatrix} u_1 \\ u_2 \end{bmatrix} \quad (9)$$

Note that at low frequencies the transfer function from fuel to pressure is approximately the same as when designing using sequential loop closing, see equation 8. Furthermore at high frequencies $\mathbf{G}^* \approx \text{diag}(G_{11}, G_{22})$.
In practice perfect decoupling is not possible due to model uncertainties. Decoupling controllers requires accurate process models and are sensitive to modelling errors, particularly when the RGA elements are large [3]. However theoretically the decoupling from u_1 (fuel flow) to y_2 (water level) can be assumed perfect. Regarding decoupling the other way problems arise in realizing $-\frac{G_{12}}{G_{11}}$ due to an improper system and the zero in the origin of G_{11}. In the frequency range of interest around the crossover frequency $-\frac{G_{12}}{G_{11}}$ is nearly constant with zero phase. For this reason $-\frac{G_{12}}{G_{11}}$ is substituted with a constant. The decoupled system is compared with the original system in the magnitude plot in figure 15.

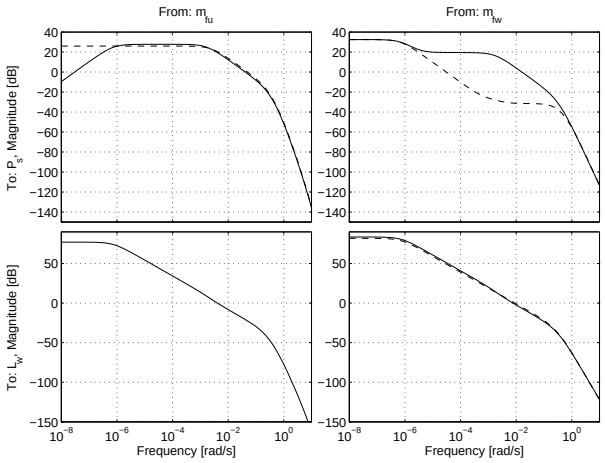

Figure 15: Comparison of open loop model without decoupling, $\mathbf{G}(s)$, solid and with decoupling, $\mathbf{G}^*(s)$, dashed.

From the figure it can be seen that for G_{11}^* the zero in the origin has disappeared. Furthermore the non perfect decoupling from u_2 to y_1 has damped the interaction at frequencies from well below the crossover frequency.
Now PI controllers are designed based on the diagonal elements in the new transfer matrix. Again these are designed to achieve the largest possible bandwidth in both loops having a phase margin of 45°. It should be mentioned that controllers with and without decoupling become very much alike, even though equation 9 is not valid, as the design focuses on the frequency band where figure 15 shows little difference between the graphs of the paired inputs and outputs. This also means that the only thing that influences whether a decoupling has any positive effect is whether the interaction amplifies the disturbance effect or not.
Bode plots of the output sensitivity functions achieved using the decoupling controller and that of the controller designed using sequential loop closing are compared in figure 16.

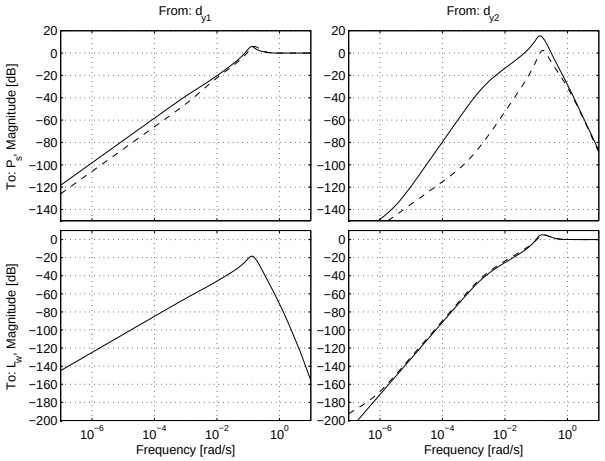

Figure 16: Comparison of sensitivity functions using sequential loop closing, solid, and decoupling design, dashed.

As the figure shows the individual sensitivities of the system based on decoupling are more damped than those based on sequential loop closing. The influence of the interactions can now be evaluated from evaluating the two controllers ability to reject disturbances on the output noting that from the specification of the normed system the objective of the controller is:

$$\|\mathbf{S}_o \mathbf{G}_{dk}\|_\infty \leq 1 \ \ \forall k$$

where $\mathbf{S}_o$ is the output sensitivity transfer matrix. $|\mathbf{S}_o \mathbf{G}_{d1}(j\omega)|$ is plotted in figure 17, that is only from the steam flow disturbance.
The plots show that decoupling has had a positive effect on the controller performance especially regarding the pressure loop. Here the resonant top using sequential loop closing is avoided at 10^{-1} rad/s and furthermore the controller actually complies with the demands.

Input Constraints

An important issue in controller design is whether input constraints cause any limit on the achievable performance. Constraints can be a problem when rejecting the transients in the disturbance.

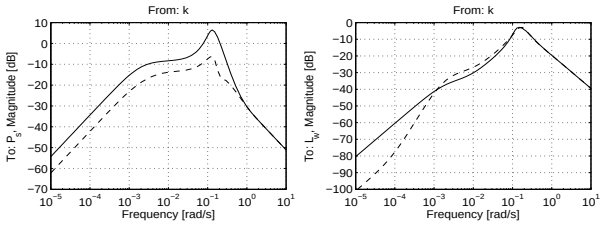

Figure 17: Illustration of effect of interaction. $|\mathbf{S}_o\mathbf{G}_{d1}(j\omega)|$ is plotted for two control strategies. Solid line is sequential loop closing and dashed line is design by decoupling.

Previous results showed that nonlinearities were concentrated in the low frequency band for which reason constraint problems as a consequence of rejecting transients in the disturbances can be carried out using linear model analysis.
This analysis can be carried out by introducing the control sensitivity $\mathbf{M} = (\mathbf{I} + \mathbf{GK})^{-1}\mathbf{K}$, describing the effect of the disturbances on the control signals. Checking whether the constraints become active can be seen from the inequality:

$$\|\mathbf{MG}_{dk}\|_\infty \leq 1 \ \forall k$$

If this inequality is violated there is not enough control signal to reject the disturbances. This reasoning of course requires a scaling of the inputs that reflects the constraints as was done previously. Again focus is limited to the steam flow disturbance. In figure 18 a plot of $|\mathbf{MG}_{d1}(j\omega)|$ is shown.

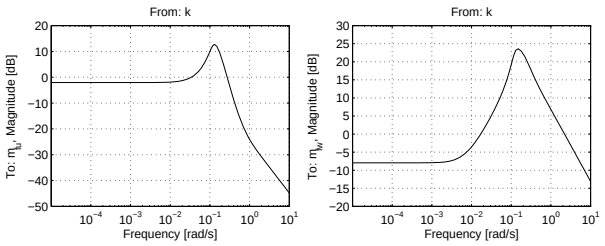

Figure 18: Plot of $|\mathbf{MG}_{d1}(j\omega)|$. The top plot represents the fuel flow and the bottom plot the feed water flow.

From this plot it is easy to see that input constraints become active for both the fuel and feed water supply.

CONCLUSIONS

This paper has shown that benefit of MIMO control can be achieved in a control strategy for the boiler system. This was a result of improved performance when decoupling the system prior to a SISO controller design.

The boiler model proved to have nonlinear behaviour mainly in the low frequency band below the crossover frequency. It was shown that one linear controller suffices leaving out gain scheduling or another nonlinear control strategy. This was manifested inspecting the performance of one linear controller to steps in the steam flow disturbance.
Input constraints showed to be a problem when controlling the boiler. This also means that the controller performance will be limited, however it is not a practical problem. The controller could be detuned to be less aggressive if the performance demands can be loosened.

Future Work

The fact that input constraints pose limitations on achievable performance, and that hard constraints for level variations are present, urge to include constraints in the controller design through an MPC strategy.
Furthermore it is of Aalborg Industries A/S' interest to introduce controllers for their boilers that do not require manual tuning and these controllers should work for a whole family of boilers. For this reason work remains in developing a strategy for making the control system self tuning. Also possible problems with model scaling should be investigated as the degree of nonlinearity and interactions in the model for scaled versions of the boiler concerned in this paper are not yet known.

REFERENCES

[1] K. Sørensen, C. M. S. Karstensen, T. Condra, N. Houbak, Optimizing the integrated design of boilers - simulation, ECOS 3 (2004) 1399–1410.

[2] B. Solberg, C. M. S. Karstensen, P. Andersen, T. S. Pedersen, P. U. Hvistendahl, Model-based control of a bottom fired marine boiler, IFAC (2005) .

[3] S. Skogestad, I. Postlethwaite, Multivariable Feedback Control: Analysis and Design, John Wiley & Sons, 1996.

[4] J. E. Rijnsdorp, Interaction in two-variable control systems for distillation columns-i, Automatica I (1965) 15–28.

[5] E. H. Bristol, On a new measure of interactions for multivariable process control, IEEE Transactions on Automatic Control AC-II (1966) 133–134.

[6] G. F. Franklin, A. Emami-Naeini, J. D. Powell, Feedback Control of Dynamic Systems, Addison Wesley Longman, 1993.